Intermittent flow behavior of random foams: A computer experiment on foam rheology

Tohru Okuzono* and Kyozi Kawasaki
Department of Physics, Kyushu University 33, Fukuoka 812, Japan
(Received 25 April 1994)

A computer experiment on foam rheology is performed with a simplified model in which the viscous dissipation in the liquid phase is taken into account. The simulation is carried out under the sheared boundary condition with a small shear rate. It is observed that violent flow like that of an avalanche occurs intermittently in the large strain regime. The distribution of energy released during avalanches and the power spectrum of the time series of energy exhibit power-law behavior. These results imply that the foam flow is understood as a self-organized critical phenomenon.

PACS number(s): 05.40.+j, 83.90.+s, 83.70.Hq

I. INTRODUCTION

Random foam systems, which have random cellular structures, exhibit a complex mechanical response known as viscoplasticity, which differs from that of a simple solid or liquid. Due to their structural complexity, analytical study of the mechanical properties, especially of the dynamical or rheological behavior of the foam systems, can hardly be performed. There are several numerical models taking cell level structures into account. Several authors have devoted much effort to obtaining the constitutive equations based upon the so-called Princen-Prud'homme model and its variants [1]. These models, however, include no randomness in their structures; that is, ordered hexagonal cells are assumed in two dimensions. Weaire and co-workers studied mechanical behavior of disorder foams [2–4], and found some interesting features on the relation between the pattern and mechanical response [5,6]. However, their model was restricted to studying the static response. Recently, Kawasaki and co-workers [7–9] proposed a dynamic model in which the structural randomness was fully taken into account. They carried out the dynamic simulation under a homogeneous shear and obtained some results that are characteristic of foam rheology, that is, the existence of finite yield stress and Bingham plasticity [9].

So far most of our attention has been directed toward studying the rheological response to homogeneous deformations in stationary states where the average flow field is externally given. Detailed flow behavior induced by a given boundary condition has never been discussed enough. We cannot, in general, expect that the homogeneous flow is always realized in a stationary state. As we will see later, such a flow field is never stationary and homogeneous. It is intermittently disordered. This dynamical behavior can be understood in a general concept of the self-organized criticality (SOC), which has been proposed by Bak, Tang, and Wisenfeld (BTW) [10,11] and which has attracted much attention over the last few years. In this paper we present the results of our computer simulation on foam rheology and illustrate the self-organized critical phenomena in our model.

II. MODEL

We use here the so-called vertex model that was proposed by Kawasaki *et al.* [12,13] to simulate coarsening of cellular patterns. In the vertex model a cellular system is described by a set of position vectors $\{\mathbf{r}_i\}$ of vertices with indices $\{i\}$. Each of the vertices is connected to three neighbor vertices by straight edges. Time evolution of the system is determined by a set of equations of motion of vertices supplemented by the elementary topological processes (see below). The vertex equations of motion are derived from the following equations of the variational form:

$$\frac{\partial R}{\partial \mathbf{v}_i}+\frac{\partial H}{\partial \mathbf{r}_i}=\mathbf{0} \quad (i=1,\ldots,N_V)\,, \tag{1}$$

where $\mathbf{v}_i$ is the velocity of the vertex i, R is the dissipation function associated with the vertex motion, H is the interfacial free energy, and N_V is the total number of vertices. For the coarsening problem R takes the quadratic form of $\{\mathbf{v}_i\}$ and H is proportional to the total edge length. Equation (1) is a force balance equation between the frictional force (the first term) and the potential force (the second term). This equation describes the slow evolution of the system for a given topology of the network of a all boundaries. In order to complete the description of the whole evolution of the system, it must be supplemented by two kinds of elementary topological processes—the so-called $T1$ and $T2$ processes. When the length of an edge becomes smaller than a small cutoff length Δ, neighbor switching ($T1$ process) or annihilation of a triangular cell ($T2$ process) occurs. These topological processes are important for the dynamics of random cellular systems [14].

A foam system, which we are concerned with here, consists of continuous (liquid) phase, the dispersed (gas)

*Present address: Department of Physics, Ochanomizu University, Tokyo 112, Japan.

phase, and the interfaces separating these two phases. The continuous phase forms a network of liquid films when the volume fraction ϕ of the dispersed phase is large ($\phi \simeq 1$). In such a situation most of the continuous phase concentrates on the junction regions of the liquid films, the so-called Plateau borders, due to the thinning property of the liquid film [15]. Bolton and Weaire [5] studied the mechanical response of a disordered two-dimensional foam with a finite fraction of the liquid phase and found that as ϕ decreases the system loses its rigidity at $\phi_c = 0.84$, which is almost the same as the random packing fraction of hard disks. However, here we restrict ourselves to studying the case $\phi \simeq 1$. In this case, each of the Plateau borders can be regarded as a vertex in our model.

In the previous study [9] we modified the vertex model to investigate the rheological behavior of foams where the viscous dissipation in the liquid phase must be taken into account. Since the dispersed phase is assumed to be filled with inviscid and incompressible gas, the viscous dissipation arises from the continuous phase, which is a viscous liquid having the shear viscosity μ. Moreover, according to the lubrication theory [16], the viscous dissipation mainly occurs near the Plateau borders. The energy dissipation rate Φ, which is associated with the extracting process of a liquid film from the Plateau border with speed U, is given by [16]

$$\Phi = 6\mu U^2 I/(3\mathrm{Ca})^{1/3} , \tag{2}$$

where I is a numerical constant having the value [17,18] $I_e \equiv 1.2215$ or $I_c \equiv 1.1866$ for $U>0$ or $U<0$, respectively, and $\mathrm{Ca} \equiv \mu|U|/\sigma$ is the capillary number. Here σ is the surface tension of single layers and is assumed to be constant over all layers and during the whole dynamical process. Using this result the dissipation function R_P associated with the viscous fluid motion is written as

$$R_P = \tfrac{6}{5}\sigma^{1/3}(3\mu)^{2/3} \times \sum_i \sum_j^{(i)} |U_{ij}|^{5/3}[I_e\theta(U_{ij}) + I_c\theta(-U_{ij})] , \tag{3}$$

with

$$U_{ij} \equiv (\mathbf{v}_i - \mathbf{u}_{ij})\cdot\hat{\mathbf{r}}_{ij} , \tag{4}$$

where the first sum in Eq. (3) is taken over the all vertices, the second sum ($\sum_j^{(i)}$) is over the three vertices j directly connected to i, $\theta(x)$ is the step function which is equal to 1 or 0 for positive or negative x, respectively, $\mathbf{u}_{ij}$ is the velocity of the fluid well inside the film, or edge, $\langle ij \rangle$, far from $\mathbf{r}_i$, and $\hat{\mathbf{r}}_{ij} \equiv \mathbf{r}_{ij}/|\mathbf{r}_{ij}|, \mathbf{r}_{ij} \equiv \mathbf{r}_i - \mathbf{r}_j$.

Since the time scale characteristic of the rheological behavior is much shorter than that which is characteristic of the coarsening of the pattern [7], a change of cell area due to the coarsening can hardly take place during a time in which rheological behavior is observed. Hence we assume that each cell area does not change in time. This condition gives rise to the constraint force terms to the vertex equations of motion in the form

$$\frac{\partial R_P}{\partial \mathbf{v}_i} + \frac{\partial}{\partial \mathbf{r}_i}\left[\sum_{\langle i,j \rangle} 2\sigma|\mathbf{r}_{ij}| - \sum_\alpha \lambda_\alpha A_\alpha\right] = \mathbf{0} , \tag{5}$$

where the first and second sums are taken over every edge $\langle ij \rangle$ and every cell α, respectively, and λ_α is the Lagrange multiplier for cell α whose area is A_α. The second and third terms in Eq. (5) are the interfacial tension and the constraint force, respectively. The Lagrange multipliers are determined from the conditions

$$\frac{d}{dt}A_\alpha = 0 \quad (\alpha = 1, \ldots, N_C) , \tag{6}$$

where N_C is the total number of cells.

The velocity $\mathbf{u}_{ij}$ in Eq. (4) still remains unknown, and some additional conditions are needed to determine $\mathbf{u}_{ij}$. It is reasonable to choose $\mathbf{u}_{ij}$, which minimizes the dissipation rate for given $\{\mathbf{v}_i\}$; that is,

$$\frac{\partial R_P}{\partial \mathbf{u}_{ij}} = 0 \tag{7}$$

for every pair of vertices ij connected by an edge. From this condition $\mathbf{u}_{ij}$ is self-consistently determined. Since $\mathbf{u}_{ij} = \mathbf{u}_{ji}$, Eq. (7) yields the following simple relation:

$$\mathbf{u}_{ij} = \tfrac{1}{2}(\mathbf{v}_i + \mathbf{v}_j) . \tag{8}$$

Equations (3)–(6) and (7) or (8) determine the vertex motion, except for the topology changes of the network structure [43].

In our previous study [9] we carried out the simulation in the case of the homogeneous shear imposed by the macroscopic velocity field $\mathbf{u}(\mathbf{r})$ at position $\mathbf{r}=(x,y)$ instead of $\mathbf{u}_{ij}$ in Eq. (4); that is,

$$U_{ij} = [\mathbf{v}_i - \mathbf{u}(\mathbf{r}_i)]\cdot\hat{\mathbf{r}}_{ij} , \tag{9}$$

where $\mathbf{u}(\mathbf{r})$ is externally imposed and given by

$$\mathbf{u}(\mathbf{r}) = \begin{bmatrix} \dot{\gamma} y \\ 0 \end{bmatrix} , \tag{10}$$

for the constant shear rate $\dot{\gamma}$. In the present model all the vertex velocities are self-consistently determined under the condition (8). Therefore, in order to simulate the flow behavior of the system, the deformations must be imposed through boundary conditions. However, we do not introduce any explicit walls at boundaries to avoid taking another dynamics between the wall and foam [1] into consideration. Here we use the following boundary conditions, which are similar to the so-called Lees-Edwards boundary conditions [19], except for the absence of the external velocity field in our model: A point $\mathbf{r}$ inside the system is identified with points $\mathbf{r}'$ at time t given by

$$\mathbf{r}' = \mathbf{r} + \Gamma(t)\cdot\mathbf{m} . \tag{11}$$

In this equation $\mathbf{m}$ represents the position of a unit system specified by a pair of integers m_x and m_y as follows:

$$\mathbf{m} \equiv \begin{bmatrix} m_x L_x \\ m_y L_y \end{bmatrix} , \tag{12}$$

where L_x and L_y are the dimensions of the unit system along the x and y axes, respectively. $\Gamma(t)$ is the shear deformation tensor which is given by

$$\Gamma(t)\equiv\begin{bmatrix}1 & \dot{\gamma}t\\ 0 & 1\end{bmatrix}. \tag{13}$$

Therefore, the velocity $\mathbf{v}(\mathbf{r})$ of the vertex located at $\mathbf{r}$ satisfies the condition:

$$\mathbf{v}(\mathbf{r}')=\mathbf{v}(\mathbf{r})+\dot{\Gamma}\cdot\mathbf{m} \tag{14}$$

with

$$\dot{\Gamma}\equiv\begin{bmatrix}0 & \dot{\gamma}\\ 0 & 0\end{bmatrix}. \tag{15}$$

Since the vertex equations of motion (5) and (6) with Eqs. (4) and (8) are Galilean invariant, that is, they are not changed by replacing $\mathbf{v}_i$ with $\mathbf{v}_i+\mathbf{u}^*$ with fixed $\mathbf{u}^*$, there is an ambiguity up to a constant velocity for every vertex. In order to avoid this ambiguity we choose the velocity $\{\mathbf{v}_i\}$ to satisfy the condition $\sum_i \mathbf{v}_i=0$ by subtracting the mean velocity of the vertices.

Intuitively, we can imagine from these boundary conditions that the two adjacent systems, which have speeds differing by $\dot{\gamma}L_y$ in the x direction, are in contact with each other. Hence the boundary conditions can introduce another length scale L_y, namely, the system size in the y direction. Indeed, in actual numerical simulations, the initial flow field contains discontinuities at $y=\pm m_y L_y$. These discontinuities, however, disappear after a short time and the homogeneous shear appears.

III. SIMULATION AND RESULTS

In order to carry out the numerical simulation using the model described in the preceding section, we write the equations of motion of vertices (5)–(7) in a dimensionless form. Here we choose $r_{\rm av}$ and $r_{\rm av}\mu/\sigma$ as the unit of length and time, respectively, where $r_{\rm av}\equiv(A/N_C)^{1/2}$ is the average linear size of cells (A is the total area of the system). In these units the equations of motion (5) and (6) are explicitly written as

$$\sum_j^{(i)} I_{ij}(U_{ij})^{2/3}\hat{\mathbf{r}}_{ij}=-\sum_j^{(i)}\hat{\mathbf{r}}_{ij}-\tfrac{1}{2}\sum_\alpha^{(i)}\lambda_\alpha\hat{\mathbf{z}}\times\mathbf{r}_{jk}$$
$$(i=1,\ldots,N_V), \tag{16}$$

$$\frac{d}{dt}A_\alpha=-\tfrac{1}{2}\sum_i^{(\alpha)}(\hat{\mathbf{z}}\times\mathbf{r}_{jk})\cdot\mathbf{v}_i=0$$
$$(\alpha=1,\ldots,N_C), \tag{17}$$

with

$$I_{ij}\equiv 3^{2/3}[I_e\theta(U_{ij})-I_c\theta(-U_{ij})], \tag{18}$$

where the sum in the second term on the right-hand side of Eq. (16) is taken over the cells that share the vertex i, $\hat{\mathbf{z}}$ is the unit vector perpendicular to the plane of cells, and j and k designate vertices of the cell α bonded to the vertex i such that (ijk) are arranged in a counterclockwise manner (Fig. 1). The sum in Eq. (17) is over the vertices belonging to the cell α.

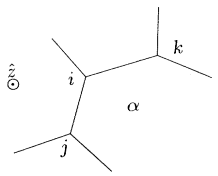

FIG. 1. Arrangement of the vertices i, j, and k belonging to the cell α. (i,j,k) are arranged in a counterclockwise manner. $\hat{\mathbf{z}}$ is the unit vector normal to the plane of cells.

We numerically solve Eqs. (16)–(18) with the self-consistent condition (8) under the boundary condition (11) or (14). The numerical technique used here is the same as that used in the previous study [9]. Initial states are obtained by the following procedure. First, we choose a cellular pattern in the scaling regime obtained by the original vertex model for the coarsening problem. Next, we relax it for enough time using the model equations described above with $\dot{\gamma}=0$. Cellular patterns thus obtained can be expected to reproduce actual random foams. We create five initial states by the method given above. The system thus obtained contain 1053, 1056, 1053, 1071, and 1064 cells. One of these initial patterns is presented in Fig. 2(a). We perform five runs with the shear rate $\dot{\gamma}=10^{-4}$, which is much smaller than the typical relaxation rate [20]. The time integrations are taken over 1.5×10^5 time steps that cover the range $0<\dot{\gamma}t<6.0$ [21]. A snapshot of the pattern during the deformation is shown in Fig. 2(b).

In order to characterize the physical state of the system at time t, we define the average density of interfacial energy, $E(t)$, and the average stress tensor $\tau(t)$ in the following:

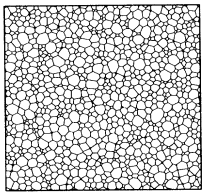

(a)

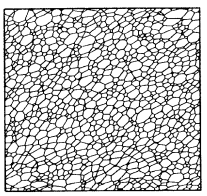

(b)

FIG. 2. Snapshots of the cellular partner. (a) The initial state at $\dot{\gamma}t=0$. (b) The deformed pattern at $\dot{\gamma}t=2.0$. The system contains 1053 cells.

$$E(t)\equiv\frac{1}{A}\sum_{\langle ij\rangle}|\mathbf{r}_{ij}|\ , \tag{19}$$

$$\tau(t)\equiv\frac{1}{A}\sum_{\langle ij\rangle}|\mathbf{r}_{ij}|\hat{\mathbf{r}}_{ij}\hat{\mathbf{r}}_{ij}\ , \tag{20}$$

where A is the total area of the system. $E(t)$ is also expressed as $\mathrm{Tr}\tau(t)$. Note that these quantities are measured in units of $2\sigma/r_{\mathrm{av}}$. In Figs. 3 and 4 $E(t)$ and shear stress $\tau_{xy}(t)$ [xy is a component of $\tau(t)$] are shown for a single run as functions of shear strain $\dot{\gamma}t$, respectively. For the small strain regime ($\dot{\gamma}t\lesssim 1$), $E(t)$ and $\tau_{xy}(t)$ monotonically increase in time, while for the large strain regime ($\dot{\gamma}t\gtrsim 1$) these quantities strongly fluctuate. In this large strain regime the energy (or stress) is intermittently released, followed by topology changes of the network structure [20]. More precisely, the energy (or stress) is homogeneously accumulated by the macroscopic deformation, and this accumulated energy (or stress) is abruptly released, followed by a sequence of topology changes. These processes are irregularly repeated. In each accumulation and release process, laminar and disordered velocity fields of cells are observed, respectively. In Fig. 5 some snapshots of the velocity field in the large strain regime are shown. In these figures dots and lines attached to them indicate the positions and velocity vectors of cells, respectively. The position of cell α is defined as $\mathbf{r}_\alpha\equiv(1/n_\alpha)\sum_i^{(\alpha)}\mathbf{r}_i$, where n_α is the number of vertices that compose the cell α and the summation is taken over such vertices. The velocity field drastically changes in a short time interval. Some vortexlike structures of the velocity field are observed. In Fig. 6 we show the displacement vectors of cells, $\{\Delta\mathbf{r}_\alpha\}$, defined as $\Delta\mathbf{r}_\alpha\equiv\mathbf{r}_\alpha(t+\Delta t)-\mathbf{r}_\alpha(t)$. Dots and lines attached to them indicate the positions of cells dna their displacement vectors, respectively. Figure 6(a) is shown for $t=2\times10^4$ and $\Delta t=0.4\times10^4$, and Fig. 6(b) for the same t but $\Delta t=0.8\times10^4$. We observe that the displacement vectors

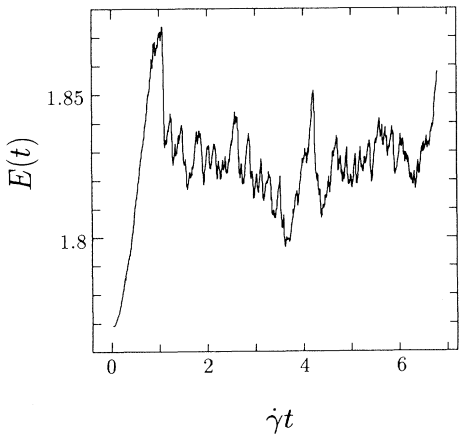

FIG. 3. The time evolution of the energy density $E(t)$. $E(t)$ is plotted as a function of shear strain $\dot{\gamma}t$ with $\dot{\gamma}=10^{-4}$. In the large strain regime ($\dot{\gamma}t\gtrsim 1$) $E(t)$ strongly fluctuates and the energy is intermittently released following topology changes of the network structure.

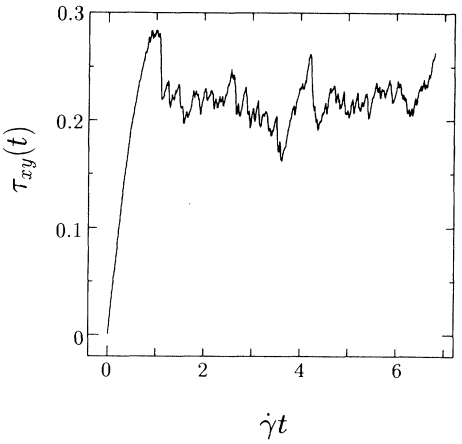

FIG. 4. The time evolution of the shear stress $\tau_{xy}(t)$, which is plotted as a function of shear strain $\dot{\gamma}t$ with $\dot{\gamma}=10^{-4}$.

also form vortexlike structures and, as Δt increases, the observed spatial structures of the displacement vector field becomes large. Unfortunately, we cannot perform a quantitative analysis of the spatial structures of the disordered flow at this stage due to a limitation of the system size, although it is an interesting problem in connection with other phenomena of disordered flow, e.g., turbulent flow of powder [22].

The dynamical behavior described above should be

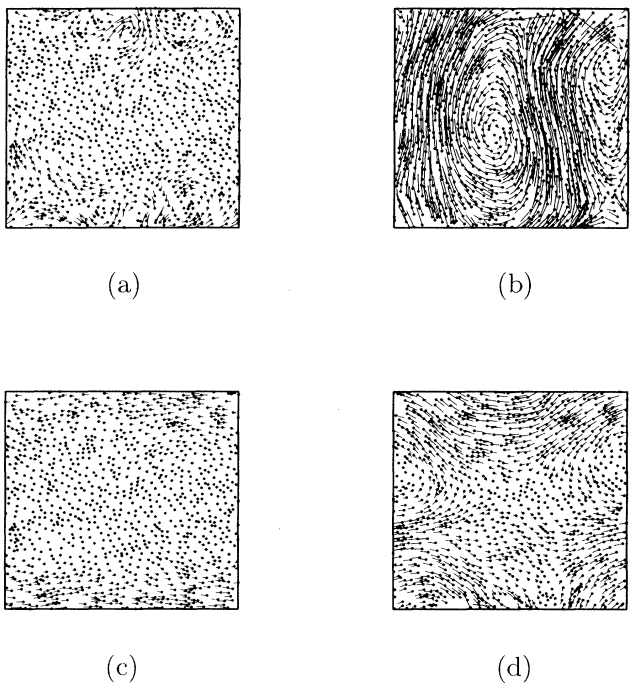

FIG. 5. Snapshots of the velocity field of cells at $\dot{\gamma}t=2.0$ (a); 2.1 (b); 2.2 (c); 2.3 (d), with $\dot{\gamma}=10^{-4}$. Dots and lines attached to them indicate the positions and the velocity vectors of the cells (arbitrary units), respectively. The velocity field is seen to change drastically in a short time interval.

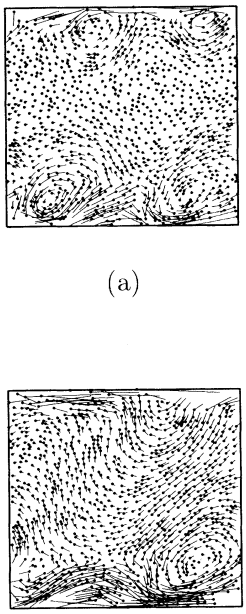

(a)

(b)

FIG. 6. Displacement vectors of cells. Dots and lines attached to them indicate the positions of the cells and their displacement vectors defined as $\Delta \mathbf{r}_\alpha \equiv \mathbf{r}_\alpha(t+\Delta t)-\mathbf{r}_\alpha(t)$ for the cell α, respectively. (The scale of the displacement vectors is the same as that of spatial coordinates. In these figures the positions of cells and their displacement vectors, which cross the system boundaries, are now drawn.) These figures are shown for $t=2\times10^4$ and $\Delta t=0.4\times10^4$ (a), and 0.8×10^4 (b). As Δt increases, the observed spatial scales of the displacement vector field increase.

compared with a stick-slip process of the earthquake models [23,24] or nonconservative cellular-automaton models [25,26] that exhibit self-organized criticality. In these models the magnitude of earthquakes or the avalanche size obey power-law behavior in the critical state [27].

Here we analyze the time series of $E(t)$ and $\tau_{xy}(t)$ in the large strain regime. We define an avalanche in a time series $\{x_n\}$ as follows, where x_n is $E(t_n)$ or $\tau_{xy}(t_n)$ at a discretized time t_n. An avalanche is an event that starts at $t=t_{n_s}$ and ends at $t=t_{n_e}$ satisfying

$$\Delta x_n < 0 \quad \text{for } n_s \le n < n_e \ , \tag{21}$$

$$\Delta x_{n_s-1}\Delta x_{n_s} \le 0 \ , \quad \Delta x_{n_e-1}\Delta x_{n_e} \le 0 \ , \tag{22}$$

where $\Delta x_n \equiv x_{n+1}-x_n$. Avalanche size s is defined as the total energy density released during an avalanche, that is, $s \equiv E(t_{n_e})-E(t_{n_s})$. In Fig. 7 the doubly logarithmic plot of the probability density $P(s)$ of the avalanche size is shown. The data are obtained from 9343 avalanches that occur in the large strain regime $2.0<\dot\gamma t<6.0$ with $\dot\gamma=1.0\times10^{-4}$ through five runs. The avalanche size obeys a power-law distribution

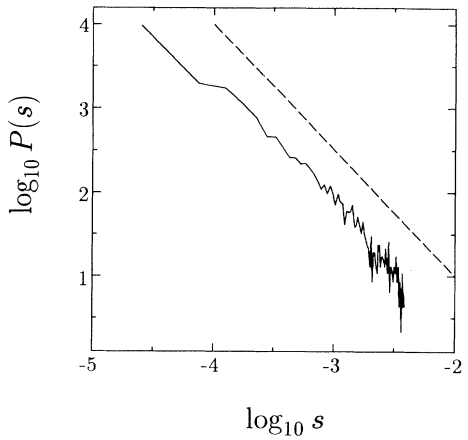

FIG. 7. Doubly logarithmic plot of the probability density $P(s)$ of the avalanche size. Avalanche size s is defined as the total energy released during an avalanche divided by the system volume. $P(s)$ appears to obey a power law. The dashed line has the slope $-\frac{3}{2}$, which is the mean-field value.

$$P(s) \sim s^{1-\tau} \ . \tag{23}$$

The exponent τ is close to the mean-field value $\frac{5}{2}$ for the sandpile model [28–30]. The dashed line in Fig. 7 indicates the slope $-\frac{3}{2}$. The same exponent is obtained in the random-neighbor model [31] for the dynamics of two-dimensional magnetic-domain patterns [32], although it shows subcritical behavior. This result should also be compared with the Gutenberg-Richter law for the size distribution of earthquakes, which says that the distribution of energy released during earthquakes obeys a power law of the Eq. (23) type with $2.25<\tau<2.5$ [33].

Feder and Feder [25] analyzed the stick-slip process in pulling sandpaper across a carpet and showed that the distribution of force jumping exerts on the sandpaper exhibits a power law. In the present case we can define a similar quantity s', which is the difference between the shear stress at the starting and ending points of an avalanche, that is, $s' \equiv \tau_{xy}(t_{n_e})-\tau_{xy}(t_{n_s})$. As we can see in Fig. 8, the probability density $P(s')$ also shows a power-law behavior with almost the same exponent as that of $P(s)$. Since in our model the vertex motions effectively exert long-range interactions due to the incompressibility of the dispersed phase, we may say that the mean-field-like behavior of this power-law distribution originates from this long-range interaction.

Next, we carry out a spectral analysis for the time series $E(t)$ and $\tau_{xy}(t)$. In the self-organized critical phenomena it is believed that the power spectrum $S(\omega)$ of the system, which responds to a small white-noise perturbation, follows a power law with the exponent φ; that is, $S(\omega)\sim\omega^{-\varphi}$. The power spectrum $S_x(\omega)$ of the time series $x(t)$ is defined as follows:

$$S_x(\omega)=\lim_{T\to\infty}\left\langle \frac{2\pi}{T}|X_T(\omega)|^2 \right\rangle \ , \tag{24}$$

$$X_T(\omega)=\frac{1}{2\pi}\int_{-T/2}^{T/2} x(t)e^{-i\omega t}dt \ , \tag{25}$$

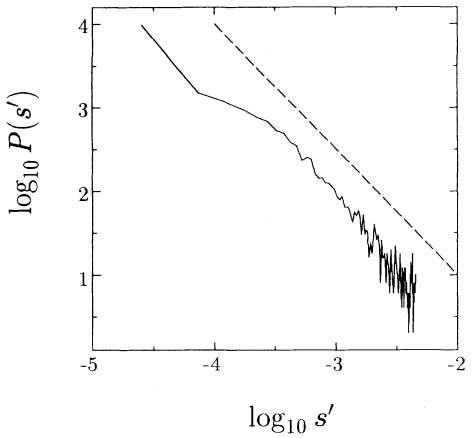

FIG. 8. Doubly logarithmic plot of the probability density $P(s')$ of the stress jump in an avalanche. $P(s')$ appears to obey a power law with almost the same exponent as that of $P(s)$. The dashed line has the slope $-\frac{3}{2}$.

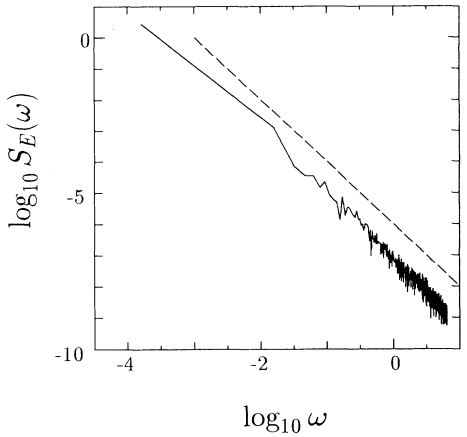

FIG. 9. Power spectrum $S_E(\omega)$ of the time series $E(t)$. $S_E(\omega)$ appears to show a power-law behavior, i.e., $S_E(\omega) \sim \omega^{-\varphi}$. The value of the exponent φ is close to 2. The dashed line has the slope -2.

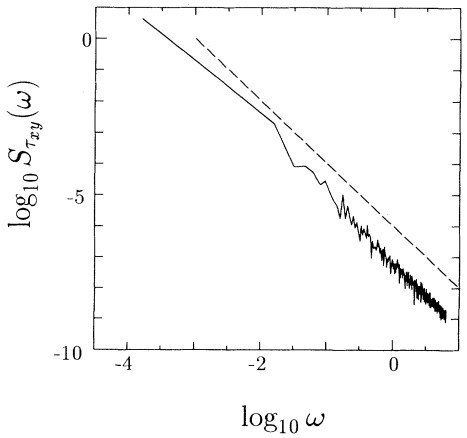

FIG. 10. Power spectrum $S_{\tau_{xy}}(\omega)$ of the time series $\tau_{xy}(t)$. $S_{\tau_{xy}}(\omega)$ appears to show a power-law behavior. The dashed line has the slope -2.

where $\langle\ \rangle$ is the ensemble average and T is a time period in which $x(t)$ is observed. In actual observation T is finite. In our present simulation, we have the time series $E(t)$ and $\tau_{xy}(t)$ for $2.0\times10^4 \le t \le 6.0\times10^4$. The ensemble average is taken over five runs. The power spectrum $S_E(\omega)$ of the time series $E(t)$ is shown in Fig. 9. We also show the power spectrum $S_{\tau_{xy}}(\omega)$ of the time series $\tau_{xy}(t)$ in Fig. 10. Both spectra exhibit power-law behavior and appear to have the same exponent $\varphi \simeq 2$ in contrast to the experimental value $\varphi \simeq 1$ by Feder and Feder. This spectrum with $\varphi = 2$, which is the spectrum of a Markov process, is observed in the experimental study of the mass fluctuations of a sandpile [34] and in the simulations of the BTW-type sandpile model [35,36]. Recently, Christensen, Olami, and Bak [37] have shown that the exponent φ depends on the level of conservation in the BTW-type model. Note that the value of φ in our simulation fluctuates around 2 by changing the time period T or the initial configuration. We need many runs and long time simulations to obtain definitive results.

IV. DISCUSSION AND SUMMARY

In our simulation presented in the preceding section, the shear rate $\dot\gamma$ is fixed at 10^{-4}. However, the avalanche size distribution $P(s)$ or the power spectrum $S_x(\omega)$ should depend on the shear rate $\dot\gamma$. They should also depend on the system size L, defined as $A^{1/2}(=N_C^{1/2})$. To examine the shear rate or system size dependence of these quantities, we have carried out additional runs for the systems which have the parameters $(\dot\gamma, N_C) = (5\times10^{-5}, 1053), (2\times10^{-4}, 1053), (1\times10^{-4}, 2067)$.

Since in the BTW-type sandpile model the avalanche size is bounded by the system size L, the average avalanche size diverges as $L \to \infty$ in the critical state [38]. In the present case the shear rate $\dot\gamma$ also restricts the avalanche size, since the avalanches cannot include all the relaxation modes slower than $\dot\gamma$. Here, it is appropriate to use the net energy $\bar s$, instead of the *density*, released during an avalanche as the site of avalanche; that is, $\bar s \equiv L^2 s$. The average size $\langle \bar s \rangle$ is defined by

$$\langle \bar s \rangle \equiv \int_0^\infty \bar s P(\bar s; \dot\gamma, L)\, d\bar s\ , \tag{26}$$

where $P(\bar s; \dot\gamma, L)$ is the probability density of $\bar s$ for fixed $\dot\gamma$ and L. We have calculated $\langle \bar s \rangle$ for each run, but we could not deduce a definitive result about the dependence of $\langle \bar s \rangle$ on $\dot\gamma$ and L, because the data are rather scattered. However, we have not observed any significant changes in the power-law behavior of $P(s)$ and $S_x(\omega)$. We believe that these power-law behaviors are essential features in our model. We conjecture that the critical state is realized in the limits $\dot\gamma \to 0$ and $L \to \infty$.

It is noteworthy that our model is rather realistic compared with other cellular automaton models or earthquake models used to study SOC, since it is based on the realistic analysis of a specific system, namely a foam under steady shear. It is interesting to determine whether real foam systems exhibit a self-organized critical behavior and how the criticality is reflected in macroscopic rheological properties. Although our model is

two-dimensional, we expect that three-dimensional systems will show at least some trace of SOC-like behavior.

Recently, an interesting experiment on pattern formation in the immiscible displacement of foam was performed by Park and Durian [39]. According to them, the pattern morphology is intimately related to rheology of foams. Here we cannot directly compare their experiment with our simulation. However, they suggest that avalanchelike rearrangement events of bubbles occur during the release of stress. This convinces us of the argument that the avalanchelike events are relevant to the rheological properties of foams. Moreover, it is hopeful that these events can be observed by means of diffusing-wave spectroscopy [40–42], because it will make quantitative discussions possible in the future.

In summary, we have carried out a computer simulation of two-dimensional foam flow under a steady shear by using the vertex model in which the viscous dissipation in the continuous phase is taken into account and the velocities of fluid motion in the liquid films are self-consistently determined. We have observed that a violent flow like that of an avalanche occurs intermittently following topology changes of the network structure. We have shown that the probability density of the avalanche size obeys a power law with approximately the same exponent as the mean field value $\tau=\frac{5}{2}$. We have also shown that the power spectrum of the time series of accumulated energy exhibits a power-law behavior with the exponent $\varphi\simeq 2$. These results give rise to the possibility that some aspects of the rheological behavior of foams can be understood with the concept of self-organized criticality.

ACKNOWLEDGMENTS

We wish to thank Professor Tatsuzo Nagia, Dr. Kazuhiro Fuchizaki, and Dr. Toshihioro Kawakatsu for valuable discussions. The computation was carried out at the Kyushu University Computer Center. This work is supported by a Grant-in-Aid for Scientific Research on Priority Areas, "Computational Physics as a New Frontier in Condensed Matter Research," and for Encouragement of Young Scientists, from the Ministry of Education, Science and Culture, Japan.

[1] A. M. Kraynik, Ann. Rev. Fluid. Mech. **20**, 325 (1988).
[2] D. Weaire and J. P. Kermode, Philos. Mag. B **50**, 379 (1984).
[3] D. Weaire, T.-L. Fu, and J. P. Kermode, Philos. Mag. B **54**, L39 (1986).
[4] D. Weaire and T.-L. Fu, J. Rheol. NY **32**, 271 (1988).
[5] F. Bolton and D. Weaire, Phys. Rev. Lett. **65**, 3449 (1990).
[6] D. Weaire, F. Bolton, T. Herdtle, and H. Aref, Philos. Mag. Lett. **66**, 293 (1992).
[7] K. Kawasaki, T. Okuzono, T. Kawakatsu, and T. Nagai, *Pattern Formation in Complex Dissipative Systems,* edited by S. Kai (World Scientific, Singapore, 1929).
[8] K. Kawasaki, T. Okuzono, and T. Nagai, J. Mech. Behav. Mater. **4**, 51 (1992).
[9] T. Okuzono, K. Kawasaki, and T. Nagai, J. Rheol. NY **37**, 571 (1993).
[10] P. Bak, C. Tang, and K. Wiesenfeld, Phys. Rev. Lett. **59**, 381 (1987).
[11] P. Bak, C. Tang, and K. Wiesenfeld, Phys. Rev. A **38**, 364 (1988).
[12] K. Kawasaki, T. Nagai, and K. Nakashima, Philos. Mag. B **60**, 399 (1989).
[13] K. Nakasima, T. Nagia, and K. Kawasaki, J. Stat. Phys. **57**, 759 (1989).
[14] D. Weaire and N. Rivier, Contemp. Phys. **25**, 55 (1984).
[15] K. J. Mysels, K. Shinoda, and S. Frankel, *Soap Films: Studies of Their Thinning and A Bibliography* (Pergamon, London, 1959).
[16] L. W. Schwartz and H. M. Princen, J. Colloid Interface Sci. **118**, 201 (1987).
[17] D. A. Reinelt and A. M. Kraynik, J. Colloid Interface Sci. **132**, 491 (1989).
[18] D. A. Reinelt and A. M. Kraynik, J. Fluid Mech. **215**, 431 (1990).
[19] M. P. Allen and D. J. Tildesley, *Computer Simulation of Liquids* (Clarendon, Oxford, 1987).
[20] T. Okuzono and K. Kawasaki, in *Trends in Statistical Physics,* Council of Scientific Research Integration, edited by J. Menon (to be published).
[21] Since we use the Euler scheme with variable time step $\delta t\equiv\min(1,\Delta/v_{\max})$, where Δ is the cutoff length for the topology change fixed at 10^{-2} and $v_{\max}$ is the maximum speed of the vertices at that time, the time of the end of simulation, t_e, fluctuates for each run. For the present runs t_e is larger than 6×10^4.
[22] Y.-H. Taguchi, Europhys. Lett. **24**, 203 (1993).
[23] J. M. Carlson and J. S. Langer, Phys. Rev. Lett. **62**, 2632 (1989).
[24] J. M. Carlson and J. S. Langer, Phys. Rev. A **40**, 6470 (1989).
[25] H. J. S. Feder and J. Feder, Phys. Rev. Lett. **66**, 2669 (1991).
[26] Z. Olami, H. J. S. Feder, and K. Christensen, Phys. Rev. Lett. **68**, 1244 (1992).
[27] Some experiments of real sandpiles show that the size distribution of an avalanches does not obey a power law and, in this case, the behavior is reminiscent of a first-order transition rather than being critical [H. M. Jaeger, C.-h. Liu, and S. R. Nagel, Phys. Rev. Lett. **62**, 40 (1989); S. R. Nagel, Rev. Mod. Phys. **64**, 321 (1992)]. However, Bretz *et al.* [M. Bretz *et al.*, Phys. Rev. Lett. **69**, 2431 (1992)] reported that the size distribution obeys a power law for smaller avalanches occurring between the large sliding events.
[28] C. Tang and P. Bak, Phys. Rev. Lett. **60**, 2347 (1988).
[29] C. Tang and P. Bak, J. Stat. Phys. **51**, 797 (1988).
[30] K. Christensen and Z. Olami, Phys. Rev. E **48**, 3361 (1993).
[31] P. Bak and H. Flyvbjerg, Phys. Rev. A **45**, 2192 (1992).
[32] K. L. Babcock and R. M. Westervelt, Phys. Rev. Lett. **64**, 2168 (1990).
[33] P. Bak and C. Tang, J. Geophys. Res. **94**, 15 635 (1989).
[34] G. A. Held, D. H. Solina II, D. T. Keane, W. J. Haag, P. M. Horn, and G. Grienstein, Phys. Rev. Lett. **65**, 1120

(1990).
[35] H. J. Jensen, K. Christensen, and H. C. Fogedby, Phys. Rev. B **40**, 7425 (1989).
[36] K. Christensen, H. C. Fogedby, and H. J. Jensen, J. Stat. Phys. **63**, 653 (1991).
[37] K. Christenesen, Z. Olami, and P. Bak, Phys. Rev. Lett. **68**, 2417 (1992).
[38] L. P. Kadanovf, S. R. Nagel, L. Wu, and S. Zhou, Phys. Rev. A **39**, 6524 (1989).
[39] S. S. Park and D. J. Durian, Phys. Rev. Lett. **72**, 3347 (1994).
[40] D, J. Durian, D. A. Weitz, and D. J. Pine, Science **252**, 686 (1991).
[41] D. J. Durain, D. A. Weitz, and D. J. Pine, Phys. Rev. A **44**, R7902 (1991).
[42] J. C. Earnshaw and A. H. Jaafar, Phys. Rev. E **49**, 5408 (1994).
[43] A new derivation of our basic vertex equations of motion without recourse to the assumption of minimum dissipation will be published in the *Proceedings of the Conference on Dynamical Systems and Chaos, Tokyo Metropolitan University, May, 1994,* edited by K. Shiraiwa *et al.* (World Scientific, Singapore, in press). The assumption of minimum dissipation is not always justified for problems far from equilibrium. Here we also point out the desirability of inventing a simpler and more elegant dynamical model system that can exhibit rich behavior similar to what we have seen in this paper.